REPORT

FRAMEWORK MATERIALS

Single-crystal x-ray diffraction structures of covalent organic frameworks

Tianqiong Ma[1,2]*, Eugene A. Kapustin[3]*, Shawn X. Yin[4], Lin Liang[1], Zhengyang Zhou[2], Jing Niu[1], Li-Hua Li[1], Yingying Wang[1], Jie Su[2], Jian Li[2], Xiaoge Wang[2], Wei David Wang[1], Wei Wang[1,5]†, Junliang Sun[2]†, Omar M. Yaghi[3,6]†

The crystallization problem is an outstanding challenge in the chemistry of porous covalent organic frameworks (COFs). Their structural characterization has been limited to modeling and solutions based on powder x-ray or electron diffraction data. Single crystals of COFs amenable to x-ray diffraction characterization have not been reported. Here, we developed a general procedure to grow large single crystals of three-dimensional imine-based COFs (COF-300, hydrated form of COF-300, COF-303, LZU-79, and LZU-111). The high quality of the crystals allowed collection of single-crystal x-ray diffraction data of up to 0.83-angstrom resolution, leading to unambiguous solution and precise anisotropic refinement. Characteristics such as degree of interpenetration, arrangement of water guests, the reversed imine connectivity, linker disorder, and uncommon topology were deciphered with atomic precision—aspects impossible to determine without single crystals.

Covalent organic frameworks (COFs) are constructed from organic building units using strong covalent bonds between light atoms (e.g., H, B, C, N, O, Si) (*1*–*3*). Progress in developing their chemistry depends on understanding their structure, but their synthesis often yields polycrystalline or amorphous products rather than single crystals. Although structures modeled from powder x-ray diffraction (XRD) have advanced the field, definitive structural solutions by single-crystal XRD (SXRD) are needed for several reasons: (i) Modeling of COF structures from powder diffraction data is difficult, especially when they are not based on the anticipated default nets (*3*, *4*); (ii) atomic positions and geometric parameters (bond lengths and angles) are usually unattainable; (iii) complexity arising from interpenetrated frameworks and disorder remains uncovered; and (iv) guest arrangement within their pores is unknown.

[1]State Key Laboratory of Applied Organic Chemistry, College of Chemistry and Chemical Engineering, Lanzhou University, Lanzhou, Gansu 730000, China. [2]College of Chemistry and Molecular Engineering, Beijing National Laboratory for Molecular Sciences, Peking University, Beijing 100871, China. [3]Department of Chemistry, University of California-Berkeley; Materials Sciences Division, Lawrence Berkeley National Laboratory; Kavli Energy NanoSciences Institute at Berkeley; Berkeley Global Science Institute, Berkeley, CA 94720, USA. [4]Drug Product Science & Technology, Bristol-Myers Squibb Co., One Squibb Drive, New Brunswick, NJ 08903, USA. [5]Collaborative Innovation Center of Chemical Science and Engineering, Tianjin 300071, China. [6]King Abdulaziz City for Science and Technology, Riyadh 11442, Saudi Arabia.
*These authors contributed equally to this work.
†Corresponding author. Email: wang_wei@lzu.edu.cn (W.W.); junliang.sun@pku.edu.cn (J.-L.S.); yaghi@berkeley.edu (O.M.Y.)

Previous work related to single crystals of COFs has been limited to either electron diffraction on small crystals (*5*–*8*), which are not amenable to SXRD, or to two studies of intrinsically nonporous organic networks held together by weak covalent bonds (*9*, *10*). Here, we report a general approach involving the use of aniline as a modulator to grow high-quality large single crystals of three-dimensional (3D) porous COFs held together by strong imine bonds (~600 kJ/mol) (*11*). Aniline has a reactivity similar to that of COF constituents, but it is monofunctional and acts as an inhibitor to nucleation, and thus alters the crystallization process. The exceptional quality of the crystallographic data collected on these crystals enabled the anisotropic refinement of a series of COFs with resolutions of up to 0.83 Å, similar to that commonly obtained for small discrete molecules (*12*).

These data allowed us to answer outstanding questions pertaining to reported COFs and also solve and refine with atomic precision the crystal structures of completely new ones. Specifically, the degree of interpenetration in imine-based COF-300 was deciphered, and the arrangement of water guests in the hydrated form of COF-300 was determined. The reversed imine connectivity for COF-303 was distinguished from the nonreversed analog, and the crystal structure of an isoreticularly expanded COF (LZU-79) was obtained. In addition, we solved and refined the single-crystal structure of a newly synthesized chiral LZU-111 with the rare *lon-b-c3* topology (*13*), which, owing to its complexity, would have been difficult to model and refine from powder XRD.

The critical step in the crystallization of COFs is the establishment of conditions for the formation of well-ordered, defect-free crystals. Such reaction conditions should be designed to allow the covalent linkage (imine in our structures) between the building blocks to be reversible, yet slow enough for efficient self-correction of defects. In a typical imine COF synthesis, the formation of amorphous solid is initially observed, and over time this material transforms into a crystalline phase through an error-correction mechanism (*8*). Thus, immediate precipitation causes the COF solid to be invariably amorphous or polycrystalline rather than single crystalline.

We sought to increase the reversibility of imine bond formation and dissociation by means of the imine-exchange strategy (*14*, *15*). This was achieved by adding a large excess of aniline to the reaction mixture, where aniline functions as a modulator (Fig. 1A). First, the reactivity of aniline is comparable to that of the building blocks used in the synthesis of most imine-based 3D COFs. Other substituted anilines (e.g., *p*-methoxyaniline, *p*-methylaniline, *o*-, *m*-toluidine, *p*-iodoaniline), produced more poorly crystalline phases or even did not produce any crystalline materials, presumably because of the mismatch of their reactivity with the amine building blocks (section S2 of the supplementary materials) (*16*, *17*). Aniline is a monofunctional molecule, so it acts as a nucleation inhibitor and competitive modulator with the multifunctional amine-based building units (*18*, *19*). Second, imine bonds are more susceptible to nucleophilic attack by amines rather than by water (*20*).

Thus, the addition of aniline increases the overall concentration of amine in the reaction, enhancing the reversibility of imine bond formation and the process of error corrections, and ultimately, crystallization (Fig. 1A). As a result of adding aniline modulator to the reaction mixture, single crystals of various imine-based 3D COFs were obtained: COF-300, COF-303, LZU-79, and LZU-111 (Fig. 1B). Notably, the crystal size of single-crystalline COFs was controlled by adjusting the amount of aniline, as exemplified for COF-300 (crystal sizes of 10 to 60 μm).

Our initial goal was to crystallize the well-known COF-300 (*21*) as a single-crystalline phase. Its tetratopic amine building block, tetrakis(4-aminophenyl)methane (TAM), was reticulated with terephthaldehyde (BDA) into a porous 3D framework (Fig. 2A). In preliminary experiments, yellow amorphous solids precipitated immediately at ambient temperature when 6 M aqueous acetic acid was added into a solution of TAM and BDA in 1,4-dioxane. After the mixture was heated at 120°C for 72 hours, polycrystals of COF-300 (~500 nm) were produced (Fig. 1B) (*17*). The reaction parameters such as time, temperature, pH, solvent, and concentration were systematically varied and optimized. However, similar to other COFs, the crystal size could not be further increased, and the crystallinity remained poor.

By using the aforementioned imine-exchange approach, in the presence of a large excess of aniline (15 equiv.), single crystals of COF-300 up to 100 μm in size were produced within 30 to 40 days

in the shape of well-defined, uniform blocks. This sharp increase in size from 0.5 to 100 μm enabled the successful SXRD data collection. By using laboratory source of x-ray, the structure of COF-300 was solved and refined with a resolution of 0.85 Å. This COF crystallized in the space group $I4_1/a$ with unit-cell parameters of $a = b = 26.2260(18)$ Å, $c = 7.5743(10)$ Å, and a unit-cell volume of 5209.6(10) Å^3. Given the default diamond topology for COF-300 and the body-centered tetragonal space group $I4_1/a$, the degree of interpenetration (N) for its structure was initially determined from the unit-cell parameters ($N = 2a/c = 7$) (*21*). The crystal structure was solved and refined anisotropically, and indeed, was sevenfold interpenetrated (*dia-c7*, class Ia of interpenetration) (*22*, *23*).

In the case of previously reported COF-300, which was made under different conditions and characterized as polycrystalline powder, the degree of interpenetration was determined to be fivefold (*dia-c5*, class Ia of interpenetration) (*21*). There was ambiguity as to the degree of interpenetration in this *dia-c5* phase, because it did not closely obey the N formula ($N = 2a/c = 4.5$). Without a single-crystal structure, the ambiguity was further deepened by the possibility of framework distortion not accounted for by the formula. In the present single-crystal structure of COF-300, these ambiguities were resolved. The sevenfold interpenetrated structure was distorted from ideal adamantane cages (natural tile for *dia* topology); the angles between the tetratopic nodes were 89.4(3)° and 120.4(3)° instead of 109.5°. In addition, the SXRD data that we collected using synchrotron source allowed for the assignment of the positional disorder of the BDA linker, a feature usually omitted during structural modeling based on powder XRD data.

We then monitored the hydration of COF-300 using SXRD measurements. Exposure of COF-300 crystals to water led to the formation of a new phase that was initially detected by measurement of the unit-cell parameters. This new phase of hydrated COF-300 adopts the same space group but with $a = b = 19.6394(9)$ Å, $c = 8.9062(4)$ Å, and a much smaller unit-cell volume of 3435.2(4) Å^3 (Fig. 2B). Despite the drastic 34% reduction in the unit-cell volume and subsequent mechanical stress on the crystal, the crystallinity of this new phase increased, enabling data collection with a resolution of 0.83 Å: a standard requirement for molecular SXRD crystallography (*12*). The hydrated COF-300 structure was solved and refined anisotropically, and the degree of interpenetration remained at 7, in stark contrast with what one would predict based on the unit-cell parameters of the hydrated form ($N = 2a/c = 4.4$). The structure was accommodated by further deviations of the angles between the tetrahedral nodes [64.4(3)° and 135.7(3)°]. Thus, the assignment of the degree of interpenetration based on the unit-cell parameters alone (as would be the case in powder diffraction) would lead to an incorrect conclusion.

The distortion in hydrated COF-300 may be caused by the presence of the strongly bound water guests at the imine functional group via the O–H···N hydrogen bond of d(O–H···N) = 3.086(7) Å, where the lone pair on nitrogen acts as an acceptor of the hydrogen bond. These water guests made infinite chains within the channels of COF-300 (Fig. 2C). The cooperative effect of hydrogen bonding within the pore led to shrinkage of the framework, which resulted in a denser structure, manifested by the increased resolution of the collected data. It was not possible to determine the nature of the host-guest interactions when the polycrystalline sample was the only available one. The hydration of COF-300 single crystals was reversible, and the macroscopic effect of hydration could be seen even in their morphology change in Fig. 1B (COF-300 versus hydrated COF-300).

To further explore imine-based 3D COF structural chemistry, we synthesized analogs of COF-300 (COF-303 and LZU-79) as large single crystals and studied them. In contrast to COF-300, COF-303 was a result of reversed imine condensation between a tetratopic aldehyde, tetrakis(4-formylphenyl)methane (TFM), and a ditopic amine, phenylenediamine (PDA) (Fig. 3A). As expected, this COF is almost identical to COF-300 in terms of its symmetry, framework geometry, topology, and degree of interpenetration, but not in its imine connectivity. Indeed, COF-300 and COF-303 were indistinguishable by powder XRD or electron diffraction. SXRD was the only technique that could detect the "switch" of this imine bond, as confirmed by the comparison of the C–C=N–C and C–C–C=N torsion angles (for both COFs) in the aniline and benzylidene moieties, respectively (Fig. 3B and table S5) (*17*, *24*).

Isoreticular expansion of COF-300 led to the formation of LZU-79, which is reticulated by

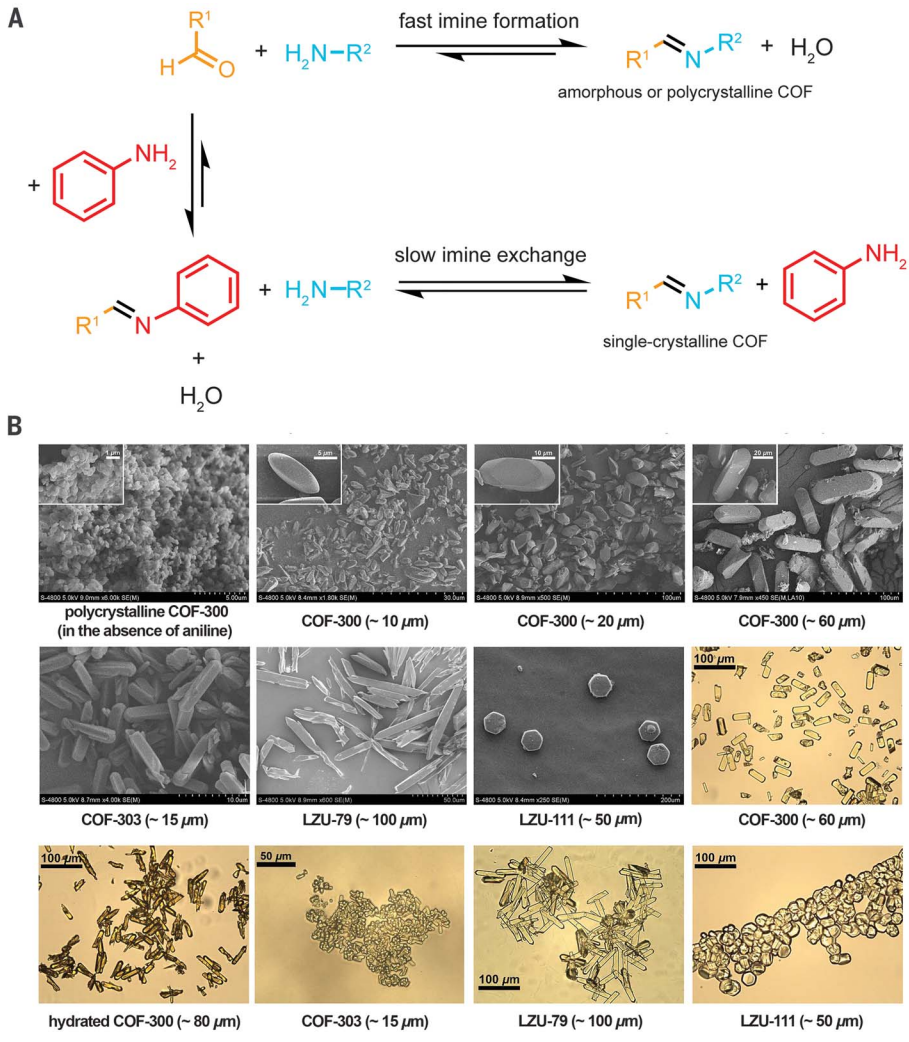

Fig. 1. Crystal growth of large imine-based COFs modulated by aniline. (**A**) In the absence of aniline, the imine-formation equilibrium is shifted toward the product, amorphous or polycrystalline COFs, whose formation is governed by fast nucleation and limited crystal growth. In the presence of aniline, the initial imine bond formation is comparably fast; however, slow imine exchange enables the growth of single-crystalline COFs. (**B**) Scanning electron microscopy (SEM) and optical microscopy images of single-crystalline COFs, obtained in the presence of aniline, the structures of which were solved and refined in this report. The SEM image of polycrystalline COF-300 without addition of aniline is shown for comparison.

tetratopic TAM and 4,7-bis(4-formylbenzyl)-1*H*-benzimidazole (BFBZ). LZU-79 crystallized in the space group $P4_2/n$ with unit-cell parameters of $a = b = 27.838(2)$ Å, $c = 7.5132(12)$ Å and a unit-cell volume of 5822.4(3) Å^3. The solved and refined SXRD structure showed that LZU-79 possessed a *dia-c10* network (class Ia of interpenetration), one of the highest degrees of interpenetration reported in COFs (Fig. 3C) (*25*).

To confirm the generalizability of our approach for growing large single crystals of COFs, we accessed a single-crystalline phase of a new chiral COF LZU-111. This COF is composed of two types of tetrahedral building blocks [methane-based tetraamine (TAM)] and [silane-based tetraaldehyde (TFS)], linked by imine bonds into a 3D chiral porous framework (Fig. 4A). Similar to COF-300 crystallization, preliminary experiments yielded only polycrystalline material. Addition of a large excess of aniline (80 equiv.) afforded single crystals of LZU-111 up to ~60 μm in the shape of well-defined hexagonal prisms within 80 days. Initially, we measured hexagonal unit-cell parameters using the data collected with a laboratory source of x-ray radiation and $a = b = 20.17(3)$ Å, $c = 34.0(3)$ Å and a unit-cell volume of 11980.4(2) Å^3.

To obtain higher resolution, we then collected the SXRD datasets with a synchrotron light source. Data resolution for single-crystal LZU-111 reached 1.2 Å, which is lower than that of typical molecular crystals (0.8 Å) but higher than that of proteins (2.5 Å). On the basis of the reflection conditions ($00l$, $l = 6n$) and Laue class ($6/m$), the space group was determined as $P6_1$ or $P6_5$. Only the positions of the relatively heavy Si atoms were located with Si–Si distances of 21.2 and 8.2 Å. The first corresponds to the shortest Si–Si distance within the four-connected network, while the second is the Si–Si distance between adjacent interpenetrating networks. Therefore, the LZU-111 topology was determined as a threefold interpenetrated lonsdaleite network *lon-b-c3* related by a threefold axis, a rare example of class IIa of interpenetration. The network is binary owing to different carbon and silicon tetrahedral nodes. This topology is rarely found in reticular chemistry of frameworks such as metal-organic frameworks (*26*) and has not been reported in COFs, precluding the correct choice of starting structural model for the accurate refinement simply on the basis of powder XRD data. Ultimately, the crystal structure of LZU-111 was fully assigned and isotropically refined in the space group $P6_5$. The chirality of LZU-111 originates from the threefold interpenetration; the intersections of the networks generates a 6_5 screw axis.

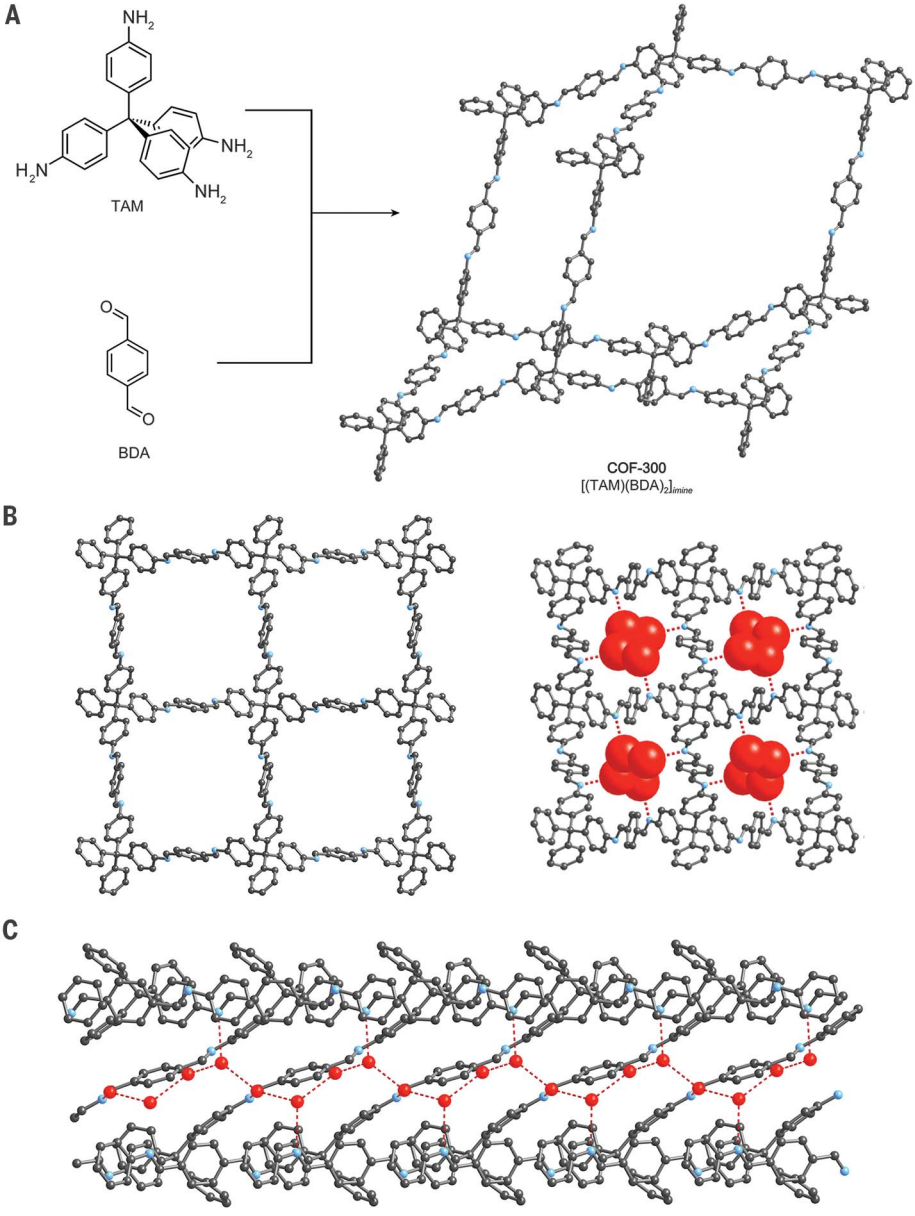

Fig. 2. Single-crystal XRD structures of COF-300 and its form containing water guests. (**A**) Imine condensation between TAM and BDA produced single-crystalline COF-300. It crystallizes in the space group $I4_1/a$ with *dia* topology and sevenfold interpenetrated framework. (**B**) Upon exposure to water, the crystal structure of COF-300 contracts substantially to form hydrated COF-300. This distortion is due to the formation of highly favorable hydrogen bonds between the imine functional groups and the water guests. (**C**) The cooperative effect of the hydrogen bonds leads to infinite chains of water guests within the channels of the framework, resulting in a much denser structure. Color scheme: C, gray; N, blue; O, red. Red dotted lines represent hydrogen bonding.

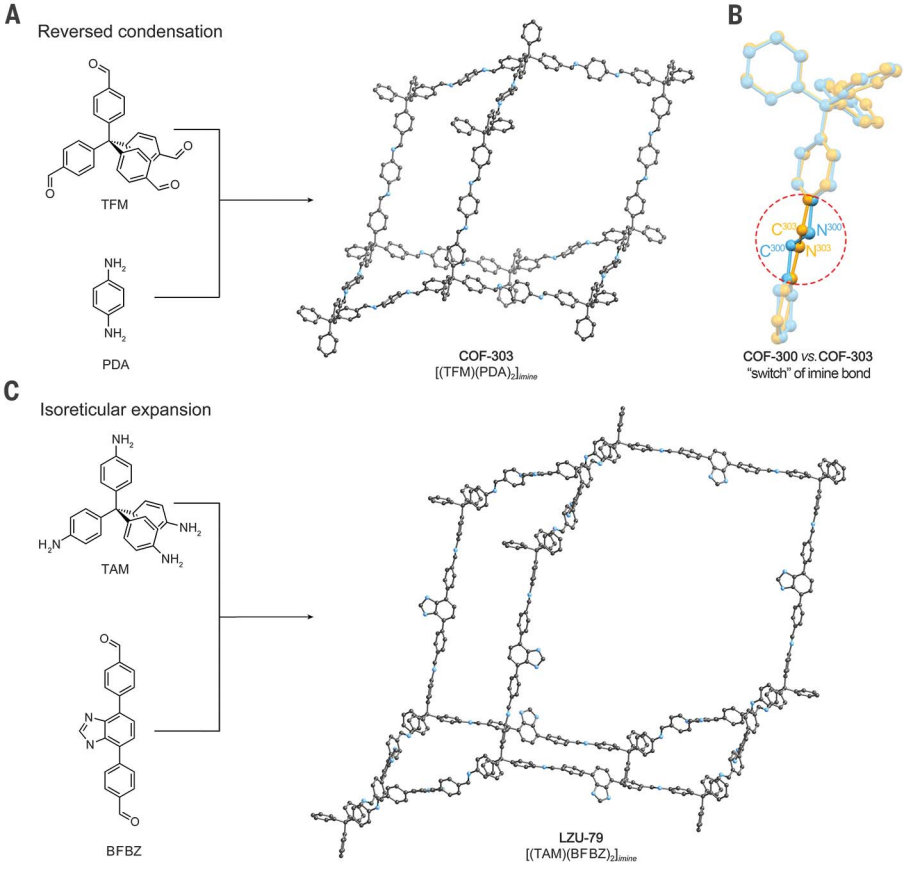

Fig. 3. Single-crystal XRD structures of COF-303 and LZU-79. (**A**) Reversed imine condensation between TFM and PDA produced COF-303. It crystallizes in the same space group as COF-300, preserving the framework geometry, the *dia* topology, and the sevenfold interpenetration. (**B**) Ball-and-stick models of COF-300 (blue) and COF-303 (yellow) are overlaid to show the only structural difference, "switched" imine connectivity, which can be distinguished from the torsion angles in the aniline and benzylidene moieties. (**C**) Isoreticular expansion of COF-300 results in LZU-79 produced by imine condensation of TAM and BFBZ. LZU-79 crystallizes in the space group $P4_2/n$. It preserves the *dia* topology but has a higher degree of interpenetration (*dia-c10*). Color scheme: C, gray; N, blue. Hydrogen atoms are omitted for clarity.

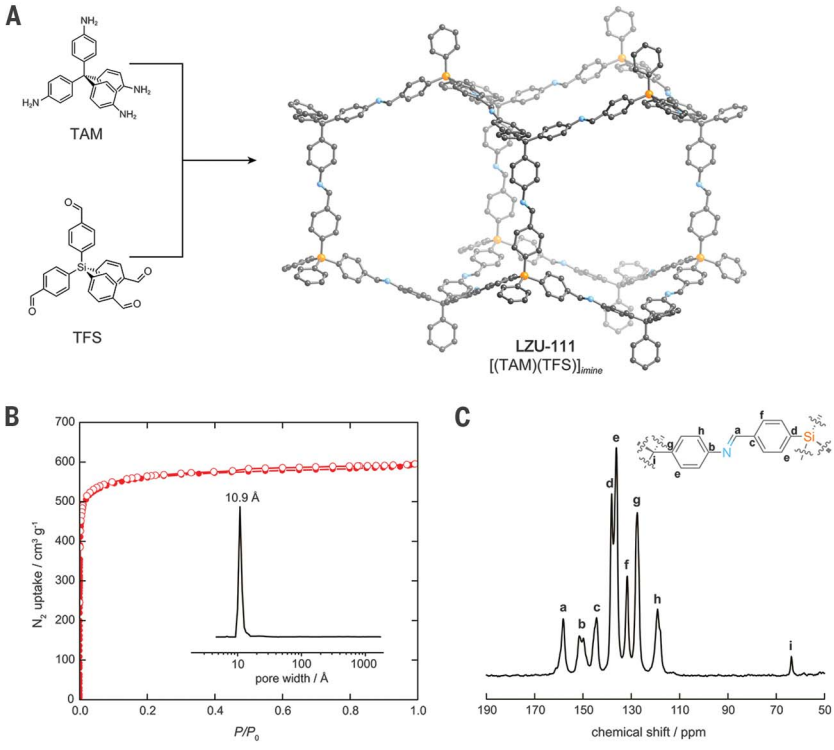

Fig. 4. Single-crystal XRD structure of chiral LZU-111 and its characterization. (**A**) Imine condensation between TAM and TFS produced LZU-111. It crystallizes in the chiral space group $P6_5$ and possesses *lon-b-c3* topology. (**B**) Activated single-crystalline LZU-111 was also characterized by nitrogen sorption at 77 K, which clearly shows a steep type I isotherm and narrow pore-size-distribution, supporting the defect-free nature of its single crystals. Solid and open circles represent the adsorption and desorption branches, respectively. (**C**) Solid-state ^{13}C CP/MAS NMR spectroscopy verified the anticipated covalent bonding at the atomic level. The ^{13}C CP/MAS NMR signals have been fully assigned: very narrow NMR signals indicate the high crystallinity and low number of defects in the structure. Color scheme: C, gray; N, blue; Si, orange.

To support the single-crystal structural refinement of LZU-111, we characterized porosity, crystallinity, and degree of defects of this new COF (Fig. 4, B and C). The nitrogen sorption isotherm at 77 K showed the classic type I isotherm with a steep uptake P/P_0 below = 0.001, characteristic for microporous materials (*27*). The experimental Brunauer-Emmett-Teller (BET) surface area of 2120 $m^2 g^{-1}$ and total pore volume of 0.918 $cm^3 g^{-1}$ are almost identical with those estimated theoretically from the SXRD model (2209 $m^2 g^{-1}$ and 0.828 $cm^3 g^{-1}$, respectively). Nonlocal density functional theory derived a narrow pore-size-distribution centered at 10.9 Å, the value of which is fully consistent with that determined from the crystal structure (~11 Å) (fig. S31) (*17*). Solid-state ^{13}C and ^{29}Si cross-polarization magic angle spinning (CP/MAS) nuclear magnetic resonance (NMR) spectroscopy verified the anticipated covalent bonding at the atomic level. The ^{13}C CP/MAS NMR signals have been fully assigned as shown on Fig. 4C. A single isotropic peak at δ = −14 parts per million (ppm) in the ^{29}Si CP/MAS NMR spectrum indicates that all the Si atoms are symmetrically equivalent, which is consistent with the SXRD analysis (fig. S20) (*17*).

REFERENCES AND NOTES

1. A. P. Côté *et al*., *Science* **310**, 1166–1170 (2005).
2. H. M. El-Kaderi *et al*., *Science* **316**, 268–272 (2007).
3. C. S. Diercks, O. M. Yaghi, *Science* **355**, eaal1585 (2017).
4. P. J. Waller, F. Gándara, O. M. Yaghi, *Acc. Chem. Res.* **48**, 3053–3063 (2015).
5. Y. Liu *et al*., *Science* **351**, 365–369 (2016).
6. Y.-B. Zhang *et al*., *J. Am. Chem. Soc.* **135**, 16336–16339 (2013).
7. A. M. Evans *et al*., Seeded growth of single-crystal two-dimensional covalent organic frameworks. *ChemRxiv* [Preprint]. 12 December 2017.
8. Y. Zhao *et al*., *J. Am. Chem. Soc.* **139**, 13166–13172 (2017).
9. P. Kissel *et al*., *Nat. Chem.* **4**, 287–291 (2012).
10. D. Beaudoin, T. Maris, J. D. Wuest, *Nat. Chem.* **5**, 830–834 (2013).
11. C. Sandorfy, in *The Chemistry of Functional Groups*, S. Patai, Ed. (Wiley, New York, 1969), vol. 3, chap. 1, pp. 5–6.
12. http://journals.iucr.org/c/services/cif/reqdata.html
13. M. O'Keeffe, M. A. Peskov, S. J. Ramsden, O. M. Yaghi, *Acc. Chem. Res.* **41**, 1782–1789 (2008).
14. M. E. Belowich, J. F. Stoddart, *Chem. Soc. Rev.* **41**, 2003–2024 (2012).
15. E. Vitaku, W. R. Dichtel, *J. Am. Chem. Soc.* **139**, 12911–12914 (2017).
16. P. T. Corbett *et al*., *Chem. Rev.* **106**, 3652–3711 (2006).
17. Materials and methods are available as supplementary materials.
18. N. Stock, S. Biswas, *Chem. Rev.* **112**, 933–969 (2012).
19. M. Calik *et al*., *J. Am. Chem. Soc.* **138**, 1234–1239 (2016).
20. E. H. Cordes, W. P. Jencks, *J. Am. Chem. Soc.* **84**, 826–831 (1962).
21. F. J. Uribe-Romo *et al*., *J. Am. Chem. Soc.* **131**, 4570–4571 (2009).
22. V. A. Blatov, L. Carlucci, G. Ciani, D. M. Proserpio, *CrystEngComm* **6**, 377–395 (2004).
23. I. A. Baburin, V. A. Blatov, L. Carlucci, G. Ciani, D. M. Proserpio, *J. Solid State Chem.* **178**, 2452–2474 (2005).
24. H. B. Bürgi, J. D. Dunitz, *J. Chem. Soc. D* **9**, 472–473 (1969).
25. X. Guan *et al*., *J. Am. Chem. Soc.* **140**, 4494–4498 (2018).
26. K. M. Patil, M. E. Dickinson, T. Tremlett, S. C. Moratti, L. R. Hanton, *Cryst. Growth Des.* **16**, 1038–1046 (2016).
27. M. Thommes *et al*., *Pure Appl. Chem.* **87**, (2015).

ACKNOWLEDGMENTS

T.M., W.W., and J.-L.S. thank Q. Zheng for advice on this project and M. Li at Shanghai Synchrotron Radiation Facility (SSRF) for assisting with the SXRD data collection at the beginning of the project. E.A.K. and O.M.Y. thank H.-B. Bürgi for discussions of structure refinement. O.M.Y. acknowledges the collaboration, input, and support of Prince Turki bin Saud bin Mohammed Al-Saud (President of KACST). The staff of beamline BL14B1 at SSRF, beamlines BL17B/BL17U of National Facility for Protein Science Shanghai (NFPS) at SSRF, and beamline I19 of Diamond Light Source are acknowledged for providing assistance during data collection. **Funding:** The authors gratefully acknowledge the financial support from the National Natural Science Foundation of China (nos. 21632004, 21425206, 21471009, and 21527803). Work performed at the Advanced Light Source is supported by the Director, Office of Science, Office of Basic Energy Sciences, of the U.S. Department of Energy under contract no. DE-AC02–05CH11231. **Author contributions:** T.M., W.W., J.-L.S., and O.M.Y. conceived the idea and led the project. T.M., S.Y., L.L., and Y.W. conducted the synthesis and crystal growth. J.-L.S., E.A.K., T.M., Z.Z., S.Y., J.S., J.L. carried out the crystallographic studies. T.M., J.N., and W.D.W. carried out the NMR measurements. T.M., L.L., Z.Z., and X.W. took the crystals images and photos. T.M., L.-H.L., and Y.W. carried out the Fourier transform–infrared measurements. E.A.K., T.M., W.W., J.-L.S., and O.M.Y. interpreted the results and wrote the manuscript. **Competing interests:** None declared. **Data and materials availability:** Crystallographic data reported in this paper are tabulated in the supplementary materials and archived at the Cambridge Crystallographic Data Centre under reference numbers CCDC 1846135 to 1846140. All other data needed to evaluate the conclusions in the paper are present in the paper or the supplementary materials.

SUPPLEMENTARY MATERIALS

www.sciencemag.org/content/361/6397/48/suppl/DC1
Materials and Methods
Supplementary Text
Tables S1 to S7
Figs. S1 to S35
References (*28*–*39*)

2 April 2018; accepted 22 May 2018
10.1126/science.aat7679

Science

Single-crystal x-ray diffraction structures of covalent organic frameworks

Tianqiong Ma, Eugene A. Kapustin, Shawn X. Yin, Lin Liang, Zhengyang Zhou, Jing Niu, Li-Hua Li, Yingying Wang, Jie Su, Jian Li, Xiaoge Wang, Wei David Wang, Wei Wang, Junliang Sun and Omar M. Yaghi

Science **361** (6397), 48-52.
DOI: 10.1126/science.aat7679

Covalent organic frameworks writ large

Covalent organic framework (COF) materials have been difficult to characterize structurally and to exploit because they tend to form powders or amorphous materials. Ma *et al.* studied a variety of three-dimensional COFs based on imine linkages (see the Perspective by Navarro). They found that the addition of aniline inhibited nucleation and allowed the growth of crystals large enough for single-crystal x-ray diffraction studies. Evans *et al.* describe a two-step process in which nanoscale seeds of boronate ester–linked two-dimensional COFs can be grown into micrometer-scale single crystals by using a solvent that suppresses the nucleation of additional nanoparticles. Transient absorption spectroscopy revealed superior charge transport in these crystallites compared with that observed in conventional powders.

Science, this issue p. 48, p. 52; see also p. 35